Journal of Alloys and Compounds 715 (2017) 404–412

Contents lists available at ScienceDirect

Journal of Alloys and Compounds

journal homepage: http://www.elsevier.com/locate/jalcom

A novel method to fabricate reinforced Ti composites by infiltration of Al (Mg) into porous titanium

Sumin Kim [a, b], Gyeungho Kim [b, **], Wooyoung Lee [a, *], Hyun-Sook Lee [a], Wonyoung Jeung [b]

[a] Department of Materials Science and Engineering, Yonsei University, Seoul 12074, South Korea
[b] Korea Institute of Science and Technology, Seoul 13679, South Korea

ARTICLE INFO

Article history:
Received 31 January 2017
Received in revised form
24 April 2017
Accepted 2 May 2017
Available online 3 May 2017

Keywords:
Titanium alloy
Intermetallic compounds
Powder injection molding
Infiltration
Mechanical properties

ABSTRACT

We present a novel method to fabricate Ti composites with in-situ formed reinforcement. Porous Ti was prepared by a metal injection molding (MIM) process, and the pores in the Ti were filled with molten Al or Al-Mg. By a simple method of infiltrating the second and/or third elements for short times (30–120 s), we obtained reinforced Ti composites having near-net shape. In particular, we observed a notable feature that the addition of Mg to the molten Al considerably improves the mechanical properties of the Ti composites. From the microstructural and elemental analysis, we found that Mg plays an important role in the enhancement of mechanical properties by preventing the growth of the brittle $TiAl_3$ phase and forming an Al(Mg) solid solution inside the pores.

1. Introduction

Titanium and titanium-based alloys are widely used for various applications in the aerospace and automotive industries, because of their high strength, good corrosion resistance, and low density (4.5 g/cm^3) [1]. However, the relatively high cost of Ti alloys, due to the complex fabrication processes, has led to numerous investigations of potentially lower-cost processes. The conventional ingot metallurgy (IM) method to fabricate Ti and Ti-based alloys suffers from high prices compared to steel and aluminum [2]. On the other hand, powder metallurgy (PM) processes offer reductions in cost and lead time in manufacturing Ti alloys, and the resultant Ti alloys have advantages such as good mechanical properties, near-net shape, and near theoretical density [3–5]. Moreover, TiH_2 powder has been used as a starting material instead of pure Ti powder because TiH_2 provides several advantages such as lower cost, lower flammability, and less tendency to oxidation compared to pure Ti [6]. However, the use of TiH_2 powder in PM is accompanied by problems such as residual hydrogen in the final product and inferior mechanical properties, including brittleness and low tensile strength [7].

For the fabrication of parts with intricate shapes, the metal powder injection molding (MIM) process has been employed to circumvent the poor formability of Ti-based alloys [8]. The MIM process can be particularly beneficial if the geometry of the desired component is complex and if the alloys have poor machinability. In addition, since the MIM process can easily be adapted for the mass production of complicated three-dimensional shapes, it further reduces the production cost [9].

For MIM, a feedstock is prepared from a mixture of the metal powders and a binder. The feedstock mixture is injected into a mold. The binder is chemically and thermally removed (via heat treatment, dissolution, or catalytic decomposition) from the resulting green body. Sintering or densification at a high temperature follows as the final step. During the sintering, the remaining binder evaporates and the structures are consolidated. The final components often have porosity, and the residual pores degrade their mechanical properties. For improved mechanical properties, full density is required and an additional hot isostatic pressing (HIP) step can be adopted. For example, the fatigue strength of Ti-6Al-4V-0.5B is enhanced up to 18% by elimination of the last 2% porosity by HIP [10]. The HIP process is usually conducted at the severe conditions of high temperature over 1000 °C and high pressure over

* Corresponding author.
** Corresponding author.
E-mail addresses: ghokim@kist.re.kr (G. Kim), wooyoung@yonsei.ac.kr (W. Lee).

http://dx.doi.org/10.1016/j.jallcom.2017.05.014
0925-8388/

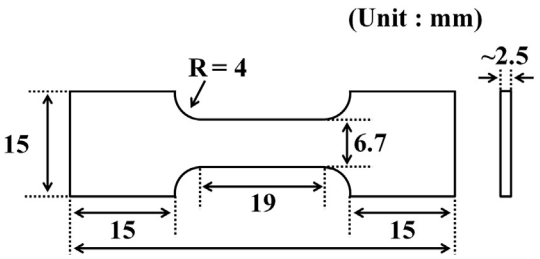

Fig. 1. Dimensions of test pieces for tensile test.

several hundred MPa for several hours. This additional densification step may negate the beneficial features of the MIM process in terms of cost and productivity.

In this study, we present a new method to fabricate reinforced Ti composites by the MIM process with a molten metal infiltration. Molten Al or Al-Mg was infiltrated into the porous Ti prepared by MIM. The resultant Ti-based composites showed a wide range of mechanical properties depending on the sintering temperature, post-heat treatment, infiltration material, and infiltration time. The effects of various processing parameters on the mechanical properties were analyzed by identifying the constituent phases and their distribution under different processing conditions.

2. Experiment procedures

To obtain the porous titanium, TiH_2 powders (>99%, −200 mesh, SE-JONG) were mixed with binders, such as polypropylene (PP), polyethylene glycol (PEG) 20000, PEG 4000, and carnauba was (CW), for 24 h by using a V-mixer. The volume ratio between TiH_2 powders and binder was 53:47, and that of binder (PP:PEG20000:PEG4000:CW) was nearly 31:55:10:4. Then the mixed powders were compacted into a green preform through extrusion and injection molding. The geometry and dimensions of a preform sintered at 1000 °C for 1 h are presented in Fig. 1. After sintering at 1000 °C for 1 h, the specimen shrinks by 25% compared to the original dimensions of the mold. In order to remove binders, solvent extraction was conducted in deionized water at 67 °C for 30 h after injection molding. Subsequently, the compacts were heated to 500 °C for 1 h under flowing hydrogen gas to burn off any residual binders, and subsequent sintering was performed in vacuum to decompose H_2 from TiH_2. In previous works, the samples pyrolyzed in H_2 showed much lower carbon residual than those in Ar, N_2, or air [11]. By this heat treatment, porous titanium was obtained. Following this process, the porous titanium was sintered at various temperatures (1000, 1100, and 1200 °C) for 1 h under vacuum (~10^{-3} Pa). To infiltrate Al (Mg) into the pores, the porous Ti was immersed into molten Al (Mg) at 730 °C for 30–120 s under Ar atmosphere. The composition of the molten Al-Mg was 80:20 wt%, respectively. Fig. 2 shows the experimental setup for immersing porous titanium in molten aluminum. After Al (Mg) infiltration, water quenching was performed to suppress the formation of intermetallic phases during cooling. For tensile testing, the specimens were mechanically polished down to grit #800 SiC paper to remove the Al(Mg) alloys attached on the surface. A post-heat treatment was employed at 1000 °C for either 10 min or for 2 h to facilitate the solid state reaction between Al (Mg) and Ti. Identical surface polishing process was applied for the tensile test to remove any potential defects on the surface of the heat treated specimens. No additional surface treatment was used for the tensile test specimens. For further densification through a solid state reaction between Al and Ti, a post-heat treatment was employed at 1000 °C for either 10 min or for 2 h.

The overall porosity and average pore diameters of the porous titanium samples sintered at the temperatures of 1000, 1100, or 1200 °C were measured using a pore size analyzer (AutoPore IV 9500). Constituent phases were identified, and their distributions were characterized, by an X-ray diffractometer (XRD; Advanced LynxEye), a field-emission scanning electron microscope (FE-SEM, JEOL, JSM 7800F), and a field-emission transmission electron microscope (FE-TEM; Talos F200X). Thin foils for TEM observation

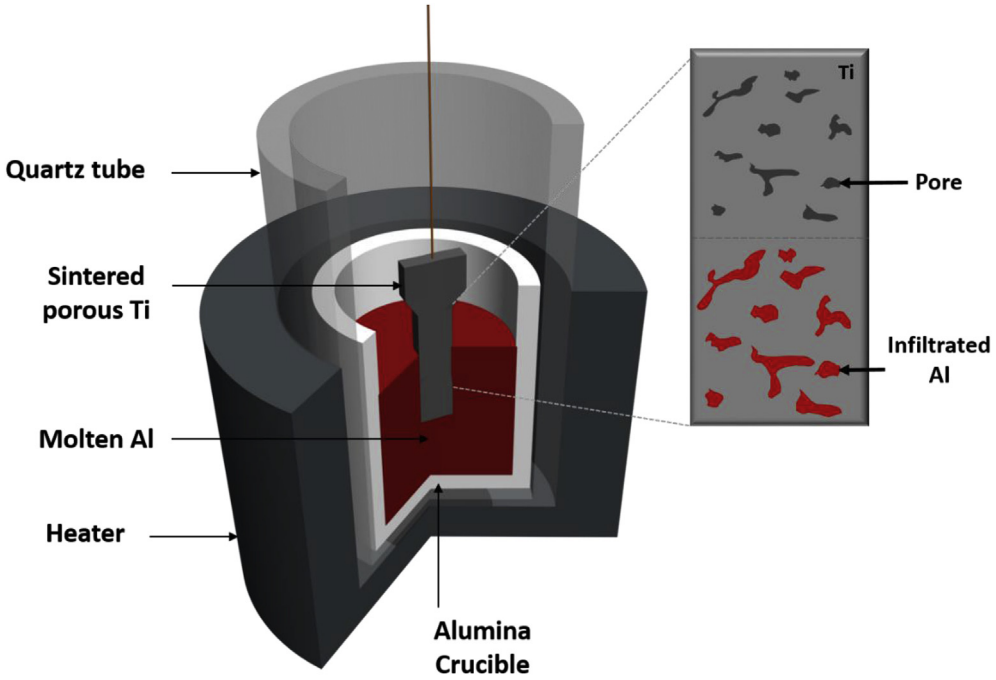

Fig. 2. Schematic of fabrication process to infiltrate Al into pores in Ti.

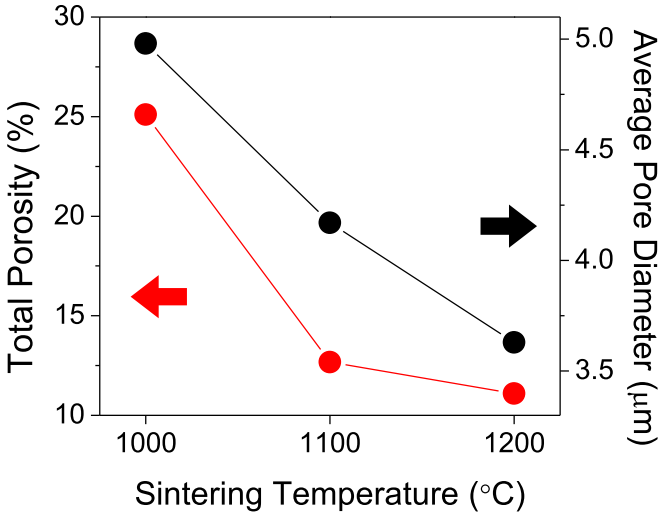

Fig. 3. Variation of total porosity and average pore diameters of porous titanium compacts prepared at different sintering temperatures of 1000, 1100, and 1200 °C for 1 h in vacuum.

were prepared by slicing with low speed diamond saw (Isomet, Buehler) and mechanical grinding and polishing down to 20 μm in thickness with SiC papers from grit 600 to 4000. Finally, Ar ion milling (Model 691, PIPS, Gatan) was employed to obtain small perforation at the center of the sample. Ion milling conditions were, 3.5 kV ion beam energy for upper and lower ion gun with sample rocking mode and beam incidence angle of 6° with typical beam current of 20 μA. An energy dispersive X-ray spectrometer (EDS) and a field-emission electron probe X-ray microanalyzer (FE-EPMA; JEOL JXA-8500F) were used for qualitative elemental analysis. The slow-strain-rate tensile (SSRT) tests were carried out at room temperature with a constant strain rate of 1×10^{-4} s^{-1} using a uniaxial tensile testing machine (Instron, 3382). After the SSRTs, the fractured surfaces of the tensile specimens were observed using the FE-SEM.

3. Results and discussion

Fig. 3 shows the total porosity and average pore diameters of porous titanium compacts prepared at sintering temperatures of 1000, 1100, and 1200 °C for 1 h. Both the overall porosity and average pore diameters decrease with increasing sintering temperature. The specimens sintered at 1000 °C show the highest values of porosity (25.1%) and average pore diameter (4.98 μm).

The porous Ti sintered at 1000 °C was used as a sample for immersion in a bath of molten Al, and the Al infiltration was conducted for various durations ranging from 30 to 120 s at 730 °C in molten Al. An excessive amount of Al infiltrated into the pores at 120s, causing the specimens to swell and deform. Therefore, the subsequent experiments were carried out for up to 90 s. Fig. 4(a) shows the SEM images of Ti compacts immersed in molten Al for 30 s. The SEM observation indicates that intermetallic compounds of Ti_xAl_y have grown within the surface of Ti pores. Fig. 4(b) shows the XRD patterns of the as-sintered sample without (0 s) and with Al infiltration (30 and 90 s). As can be seen in Fig. 4(b), the $TiAl_3$ phase appeared after Al infiltration, and its amount increases with increasing infiltration time. In addition, unreacted Al is also found as a minor phase.

The microstructural and compositional analyses of the specimens after Al infiltration were performed using FE-TEM. Results of the TEM observations are given in Fig. 5 for the sample that had been infiltrated for 30 s. Fig. 5(a)–(c) represent the high-angle-

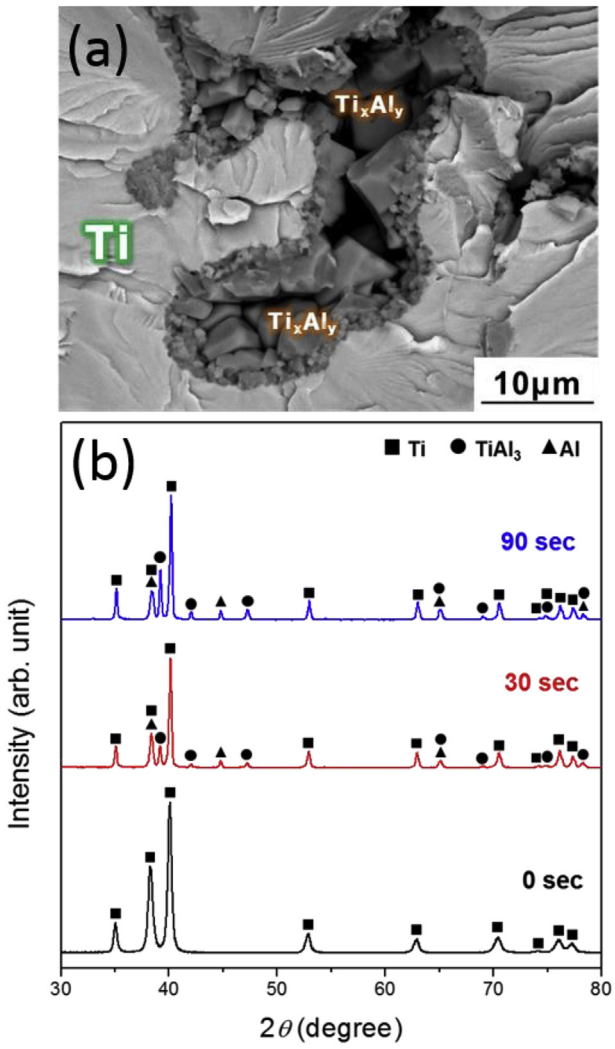

Fig. 4. (a) SEM images of titanium compacts immersed in molten aluminum at 730 °C for 30 s, and (b) XRD patterns of specimens after Al infiltration for 0, 30, and 90 s.

annular-dark-field scanning transmission electron microscopy (HAADF-STEM) image and the corresponding energy-dispersive X-ray spectroscopy (EDS) elemental mapping, respectively. The phases and compositions were crosschecked at the three selected areas that are indicated with yellow boxes in the HAADF-STEM image of Fig. 5(a), using EDS. The EDS results indicate that the main phase of intermetallic compound is $TiAl_3$ and it is formed inside the pore as well as at the interface of the pore. In addition, the Al phase unreacted with Ti exists only inside the pore, while the outside of the pore consists of pure Ti. The inset of Fig. 5(a) shows an electron diffraction pattern in a selected area at the interfacial region for the incident beam direction of [010]. The pattern clearly illustrates that the crystal possesses a tetragonal structure ($I4/mmm$) of $TiAl_3$, which is consistent with the previous report [12]. According to the calculation of Gibbs free energies of formation for different types of Ti-Al intermetallic compounds, $TiAl_3$ is the most stable phase in the temperature range of 0–1000 °C, compared to TiAl and Ti_3Al [13,14]. Therefore, it seems reasonable that the first diffusion reaction product between solid Ti and molten Al is $TiAl_3$. This is in agreement with other experimental results that have reported that $TiAl_3$ forms and remains as long as Al exists in system [13,15,16].

The growth rate of Ti-Al intermetallic compounds in the porous Ti after Al infiltration was investigated as a function of the sintering

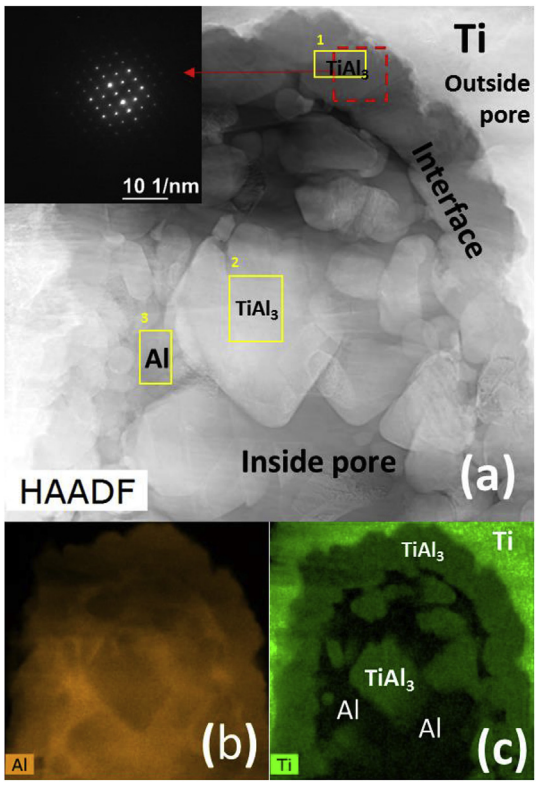

Fig. 5. FE-TEM characterization of the specimen after Al infiltration for 30 s (a) HAADF-STEM image and (b)–(c) corresponding EDS elemental maps. The inset in (a) shows an electron diffraction pattern of the selected area indicated with a red box in the main figure of (a), which was obtained for the incident beam direction of [010] $TiAl_3$. (For interpretation of the references to colour in this figure legend, the reader is referred to the web version of this article.)

temperature of the Ti compact and the immersion time in the molten Al. For this, the elemental distribution was obtained by FE-EPMA X-ray mapping in various as-infiltrated samples. As-infiltrated specimens were prepared with different infiltration times (30 and 90 s) after sintering at different temperatures (1000 and 1200 °C). The back-scattered electron (BSE) images and their elemental color mapping images for Al and Ti are presented in Fig. 6. The growth of the intermetallic Ti-Al phase inside the pores, which is initiated by Al infiltration, is clearly observed in Fig. 6. The color map images indicate that the phases formed at the pores are mainly Al-rich intermetallic Ti-Al compounds. The amount of intermetallic compounds and the Al concentration are higher at lower sintering temperatures and/or longer infiltration time conditions.

The mechanical properties of the porous Ti alloys without and with Al infiltration were analyzed by measuring tensile strength under a slow strain rate at room temperature. The SSRT results of the tensile stress-strain curves for the as-infiltrated specimens sintered at 1000 and 1200 °C are presented in Fig. 7(a) and (b), respectively. Porous Ti sintered at different temperatures showed similar behavior with Al infiltration time. At 30 s infiltration time, an increase in ultimate tensile strength (UTS) by a factor of about 2–2.5 was obtained with a slight decrease in elongation (EL). On the other hand, both UTS and EL decreased considerably as the infiltration time increases to 90 s. At the higher sintering temperature of 1200 °C, both UTS and EL are enhanced compared with samples sintered at 1000 °C in as-sintered and Al infiltrated conditions. Consequently, the highest values of UTS and EL are shown in the composite sample with 30 s infiltration after sintering at 1200 °C [Fig. 6 (c)] and the lowest values of UTS and EL appeared in the composite sample with 90 s infiltration after sintering at 1000 °C [Fig. 6 (b)]. The elemental mapping images shown in Fig. 6 imply that the better mechanical properties of the samples sintered at 1200 °C are caused by the lower porosity and smaller pore diameter that result from greater densification of porous Ti at higher sintering temperature. On the other hand, the inferior mechanical properties of the samples immersed in Al for the longer time of 90 s after sintering at 1000 °C can be interpreted as the result of extensive formation of interconnected, brittle $TiAl_3$ phase that is distributed throughout the entire sample. As already shown in Fig. 3, this sample has higher porosity and larger pore diameter, favorable for extensive formation of $TiAl_3$. From the microstructural analysis and mechanical property evaluation, it is worth mentioning that significant improvement in strength is achieved at shorter infiltration time (30 s) even with the brittle byproduct formed preferentially at the interface of the Ti pores. This suggests that further strength improvement of Ti composite is possible by molten metal infiltration by assuring the suppression of reaction product formation.

Fractographic analysis was performed to identify the origin of tensile failure. Fig. 8 shows the SEM images of the fractured surface after SSRT testing. Fig. 8(a) clearly shows that the crack is initiated at the region of $TiAl_3$ and propagates through Ti to nearby $TiAl_3$ regions along the tensile direction as indicated in the image. In addition, the magnified view of Fig. 8(b) implies that the phases of Ti and $TiAl_3$ exhibit cleavage and intergranular type fracture, respectively. Therefore, it seems reasonable that, as the amount of intermetallic $TiAl_3$ phase increases, the mechanical properties become worse as exemplified in the case of 90 s infiltration duration of the sample sintered at 1000 °C, in which the intermetallic phases are extensively formed and distributed.

In order to modify the intermetallic phase through solid-state diffusion of Al and/or Ti, post-heat treatment was performed at 1000 °C for 10 min and also for 2 h, using samples of Ti composite prepared by sintering at 1000 °C that had been Al-infiltrated for 30 s [Fig. 6(a)]. The FE-EPMA X-ray mapping images of the post-heat treated samples that were held at 1000 °C for 10 min are shown in Fig. 9(a). Likewise, Fig. 9(b) shows the corresponding results for the samples that were held at 1000 °C for 2 h. With the increasing time of post-heat treatment, the intermetallic phases grow rapidly [in as little as 10 min, as shown in Fig. 9(a)] as compared with the as-infiltrated sample [Fig. 6(a)]; eventually, after 2 h, a homogeneous intermetallic phase is formed as shown in Fig. 9(b). The microstructural changes during post-heat treatment can be explained by the diffusion of Al from the Al-rich intermetallic phase into Ti, and the consequent formation of a Ti-rich intermetallic phase at the later stage. In addition, many voids are also found, as shown in Fig. 9(b).

The voids can be generated by several routes such as (i) the melting/evaporation of Al, (ii) the Kirkendall effect from solid state diffusion, and (iii) the difference in molar volumes between reactants and products. By heating the sample at 1000 °C, which is well over the melting point of Al (660 °C), unreacted Al can be evaporated, leaving voids. The Kirkendall effect is caused by the difference of diffusion rates between Ti and Al. The diffusion rate of Al is faster than that of Ti. [17–19]; hence, Al can diffuse into the Ti phase leaving vacancies whereas Ti can hardly diffuse into the Al or $TiAl_3$ phases. For these reasons, pores initially filled with Al can be emptied after prolonged annealing at high temperature. Yi et al. [20], reported that the molar volume ratio of the reactants (Ti and Al) and products (Ti_xAl_y) is 0.932 for $TiAl_3$, 0.911 for TiAl, and 0.969 for Ti_3Al. This suggests that the formation of Ti_xAl_y intermetallic compounds from Al + Ti mixtures is accompanied by a volume contraction of about 3–9%.

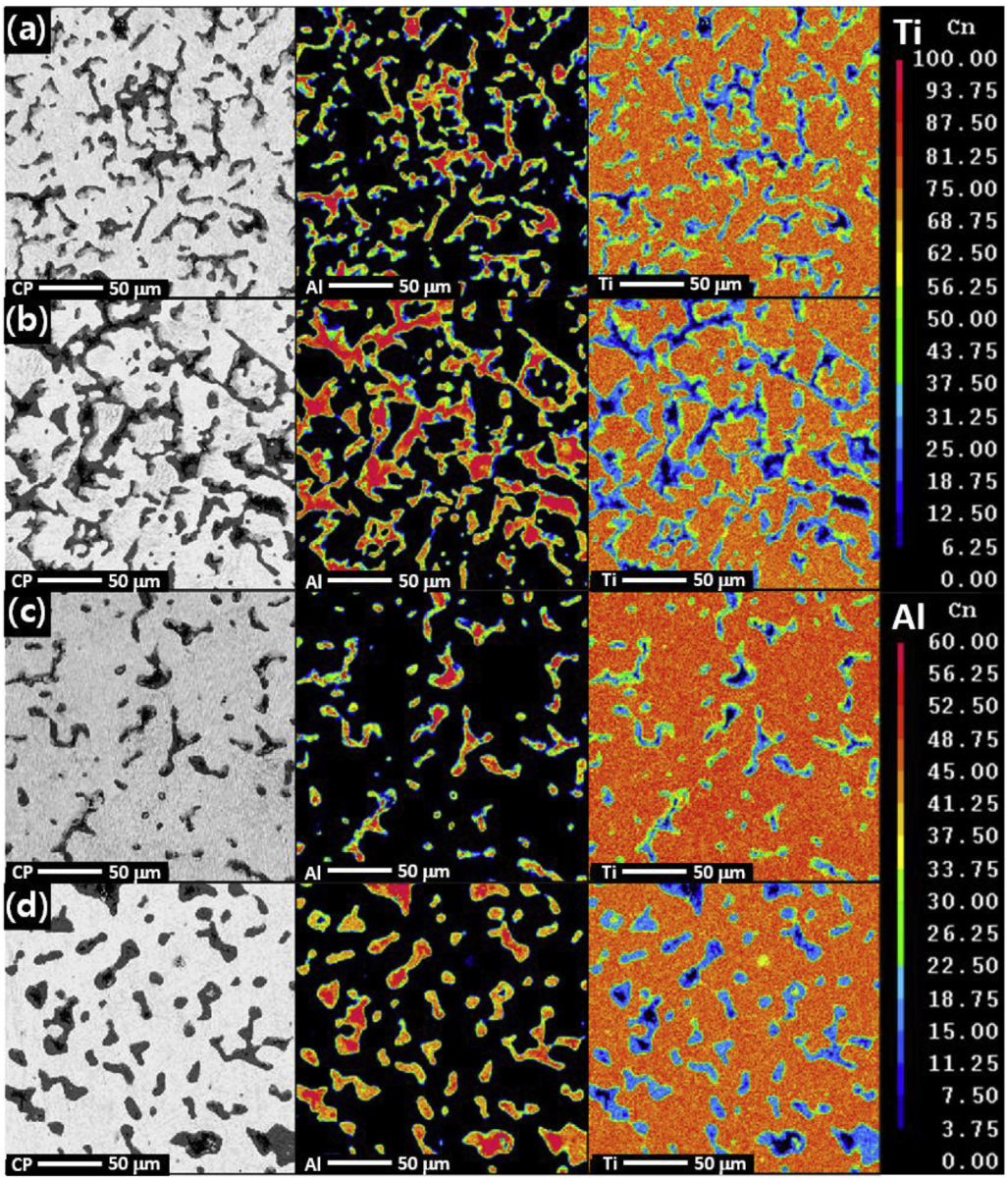

Fig. 6. FE-EPMA X-ray images, BSE images, and elemental color mapping images for Al and Ti from as-infiltrated specimens with different infiltration times (30 and 90 s) after sintering at different temperatures (1000 and 1200 °C) [(a) 30 s–1000 °C, (b) 90 s–1000 °C, (c) 30 s–1200 °C, and (d) 90 s–1200 °C].

The SSRT results of the post-heat treated specimens are shown in Fig. 10(a) for the different heating times and temperatures. The samples that had been subjected to post-heat treatment were compared with the as-infiltrated sample and showed deterioration of tensile strength and elongation. Both heat treatment temperature and holding time had adverse effects on the mechanical properties. This results from the increased amount of brittle intermetallic compounds as well as voids in the sample introduced by high-temperature heat treatment. In an attempt to remove the voids by densification, heat treatment was carried out at higher temperatures of 1100 and 1200 °C for 2 h. However, this treatment had an even more adverse effect on the mechanical properties as shown in Fig. 10(a). The SEM images in Fig. 10(b)-10(d) reveal that only coarsening took place, giving rise to the larger grains and voids. In summary, both infiltration of molten Al to porous Ti preforms and subsequent post-heat treatment processing can lead to monolithic Ti_xAl_y microstructures with stable pores; these samples exhibit intrinsically low strength and brittleness, and this result is in agreement with many attempts to fabricate intermetallic Ti_xAl_y parts through reaction and solid state diffusion. Only a few successful results have been reported and in these cases, extensive thermo-mechanical treatments with applied pressure at high temperatures were employed to eliminate residual porosity. One important conclusion drawn from this study is that once $TiAl_3$ is formed by the reaction of molten Al and solid Ti at an interface, the adverse effects on mechanical properties are persistent in spite of various post-heat treatments. A more reasonable approach for enhancing the properties of composites is to suppress the reaction between Al and Ti while ensuring the fast infiltration, i.e. adding an alloying element that has a low wetting angle and low melting point, and also does not react with Ti. One such metal satisfying the aforementioned requirements is magnesium [21,22].

As an alternative way to improve the mechanical properties, infiltration with Al-Mg alloys was conducted. The porous Ti

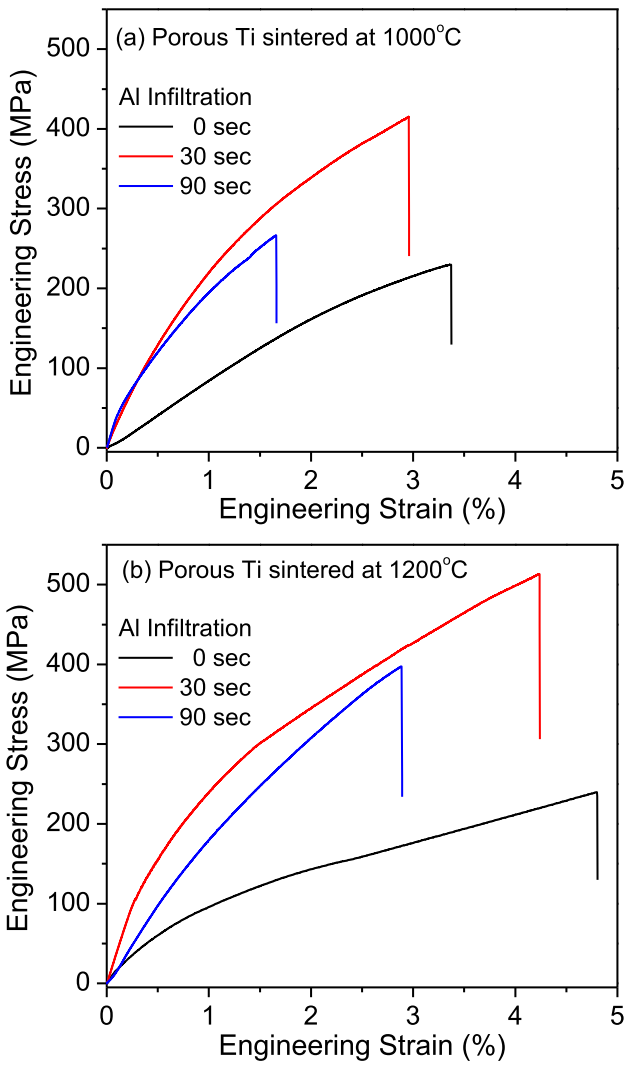

Fig. 7. Tensile engineering stress-strain curves of as-infiltrated specimens with different infiltration times (0, 30, and 90 s) after sintering of porous Ti at different temperatures [(a) 1000 °C and (b) 1200 °C].

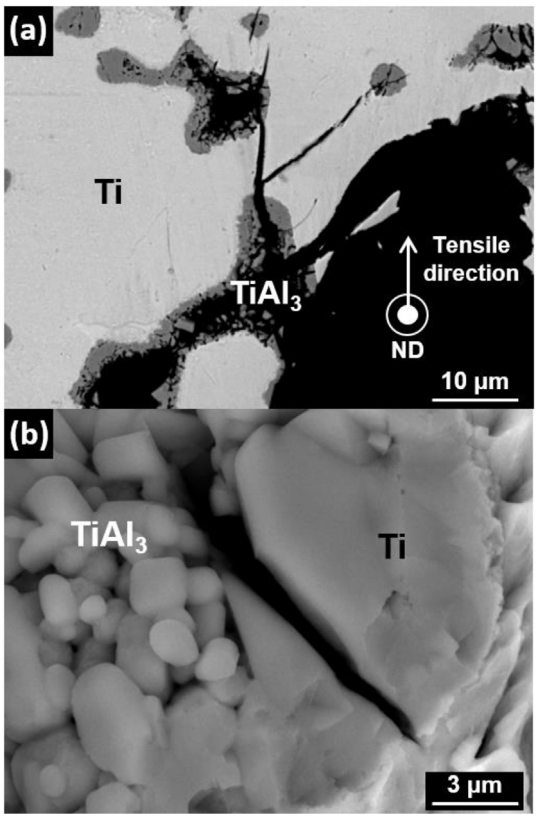

Fig. 8. (a) SEM images of the fractured surface after tensile testing, and (b) magnified view of (a).

sintered at 1000 °C was immersed in a graphite crucible containing molten Al (80 wt%)–Mg (20 wt%) for 30 and 90 s at 730 °C. At 450 °C, Mg has a 17.4 wt% solubility limit with Al. However, for the practical production of the Al-Mg alloy ingot and infiltration process, we have limited the maximum amount of Mg in the melt to about 20 wt% to avoid excessive fuming of Mg. Fig. 11(a) shows a BSE-SEM image of the specimen after Al-Mg infiltration for 90 s; while Fig. 11(b)–11(d) show the corresponding EDS elemental color mapping images for Ti, Al, and Mg. According to the EDS mapping images [Fig. 11(b)–11(d)], the nucleation of $TiAl_3$ takes place only in the narrow region at the interface of pores, and an alloy of Al and Mg fills the pores. The pure Ti, $TiAl_3$, and Al-Mg alloy are indicated with the shades of light gray, gray, and dark gray, respectively, in the BSE image in Fig. 11(a).

Fig. 12 shows the XRD pattern of the sample that was infiltrated with Al-Mg for 90 s and then quenched. The XRD peaks are indexed as the phases of Ti, $TiAl_3$, and Al(Mg) solid solution. The Al(Mg) solid solution is evidenced by the shift of the Al peaks to lower angles, indicating that the lattice parameter of Al is increased by the insertion of Mg. Other binary and ternary crystalline compounds such as Al-Mg, Ti-Mg, and Ti-Al-Mg are not observed within the detection limit of XRD. In our case, rapid cooling (water quenching) was employed to suppress the formation of $TiAl_3$ during cooling. As a result, it is reasonable to assume that ternary compound formation and any precipitation phases were kinetically unfavorable. The amounts of $TiAl_3$ phase formed by infiltrating Al and Al-Mg alloy for 90 s were estimated by the Rietveld refinement method using the XRD data in Figs. 4(b) and 12, respectively. The amount of $TiAl_3$ is 19.6 wt% with pure Al and reduces to 10.1 wt% with Al-Mg alloy infiltration; this implies that the formation of the $TiAl_3$ phase is significantly suppressed by Al-Mg alloy infiltration. The reaction formula of $TiAl_3$ is as follows:

$$Ti\ (solid) + 3Al\ (liquid) \rightarrow TiAl_3\ (solid)$$

Ideally, pure Al has an activity of 1. When alloyed, depending on the amount of Mg mixed in the solution, the activity of Al decreases because of the mixing effect. The production rate of $TiAl_3$ decreases because of the reduction of this driving force. In summary, the addition of Mg in Al effectively slows down the $TiAl_3$ formation during infiltration process by creating an Al(Mg) solid solution, which in turn, lowers the reactivity with Ti.

The SSRT results of the tensile stress-strain curves for the Al-Mg infiltrated specimens with different immersion times (30 and 90 s) from porous Ti preforms sintered at 1000 and 1200 °C are shown in Fig. 13(a) and (b), respectively. It is interesting to note that even though similar strengthening behavior is obtained from the Al-Mg alloy with a short infiltration time, further increases in both strength and elongation are noticeable in the case of the samples with longer infiltration time and higher sintering temperature. This behavior is the opposite of the pure Al infiltration case where loss of strength and elongation was found after prolonged infiltration time.

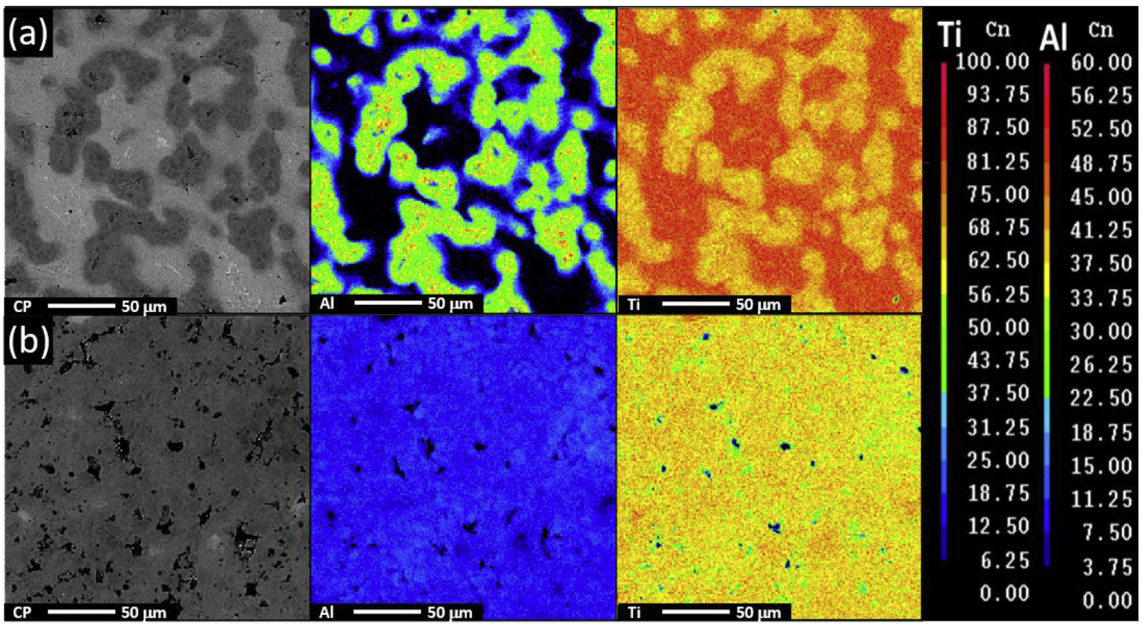

Fig. 9. FE-EPMA X-ray images, BSE images, and elemental color mapping images for Al and Ti from the specimens subjected to the post-heat treatment at 1000 °C for (a) 10 min and (b) 2 h in the case of samples subjected to Al infiltration for 30 s into the porous Ti compact that had originally been sintered at 1000 °C for 1 h.

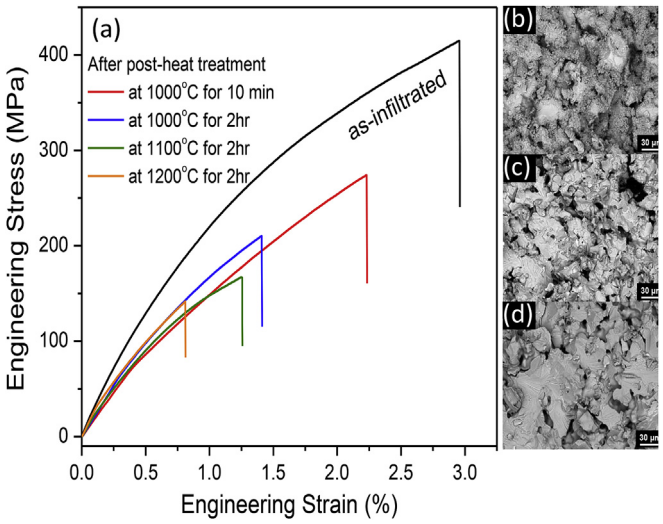

Fig. 10. (a) Tensile engineering stress-strain curves of the specimens after post-heat treatment for 10 min at 1000 °C and for 2 h at 1000, 1100, and 1200 °C in comparison with the as-infiltrated specimens with an infiltration time of 30 s. SEM images for the post-heat treated samples that were subjected to temperatures of (a) 1000, (b) 1100, and (c) 1200 °C for 2 h.

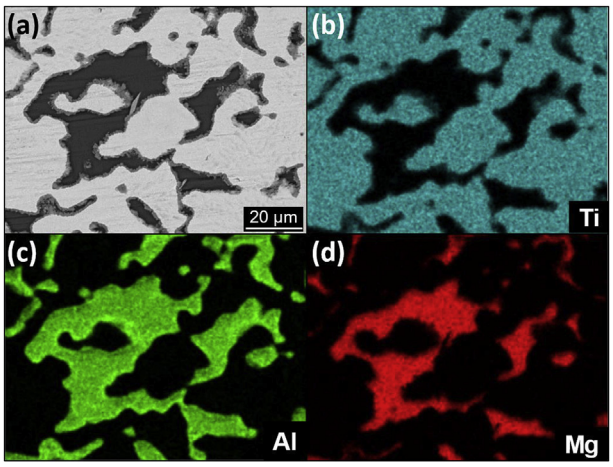

Fig. 11. (a) BSE image of FE-SEM; and EDS elemental color mapping images for (b) Ti, (c) Al, and (d) Mg of the specimen after Al(80 wt%) – Mg(20 wt%) infiltration for 90 s into the porous Ti sintered at 1000 °C for 1 h.

In order to elucidate the role of Mg addition on the mechanical properties of the as-infiltrated samples, the values of UTS and EL are compiled from the SSRT curves in Fig. 7 for pure Al and from Fig. 13 for Al-Mg. The results are presented in Fig. 14(a) and (b), respectively. Again, an apparent difference is shown for the longer immersion time of 90 s, i.e., a significant increase in both UTS and EL is achieved from the Al-Mg alloy but the opposite trend is found from the sample that had been infiltrated with pure Al. With different materials of infiltration, the major difference in the mechanical properties appears at an infiltration time of 90 s: enhancement for Al-Mg infiltrated samples but reduction for Al infiltrated samples in both UTS and EL. An excellent UTS of 750 MPa with an elongation of 7% was achieved in the case of the sample consisting of a Ti preform sintered at 1200 °C that was subsequently infiltrated with Al-Mg alloy for 90 s. The major reasons for the enhancement of mechanical properties are: i) high temperature sintering of the Ti compact for low porosity, ii) fast infiltration of molten metal for the densification of the porous Ti compact, and most importantly, iii) suppression of brittle $TiAl_3$ formation at the pore surfaces by the formation of an Al(Mg) solid solution. It should be mentioned that the Al(Mg) solid solution phase produced in this study by quenching can be additionally strengthened by proper post-aging heat treatment, and the strength and ductility of the resulting Ti-Al(Mg) composite may be further enhanced. Detailed investigations of the dominant strengthening mechanisms in this composite material, process optimization, and precipitation hardening schemes (optimum alloy composition and post-heat-treatment schedule) will be the subject of future work.

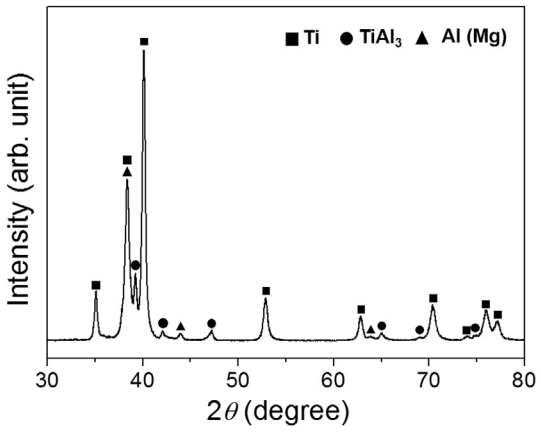

Fig. 12. XRD pattern of the specimen after Al(80 wt%) – Mg(20 wt%) infiltration for 90 s into the porous Ti sintered at 1000 °C for 1 h.

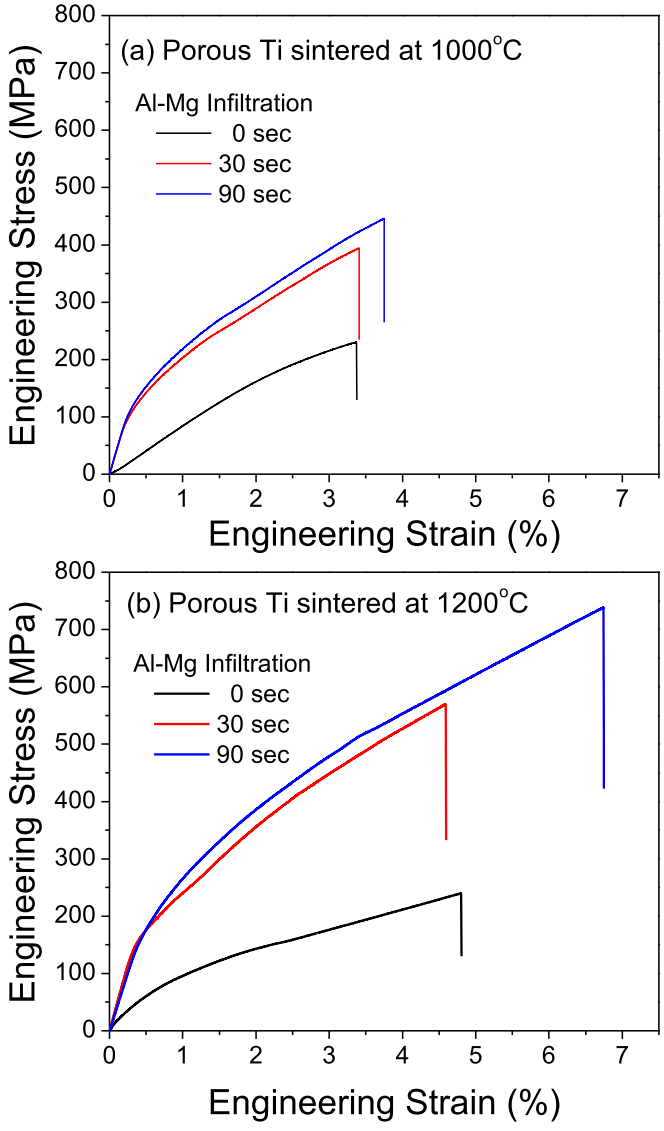

Fig. 13. Tensile engineering stress-strain curves of Al-Mg infiltrated specimens that had been sintered at different temperatures [(a) 1000 °C and (b) 1200 °C], followed by different infiltration times (0, 30, and 90 s).

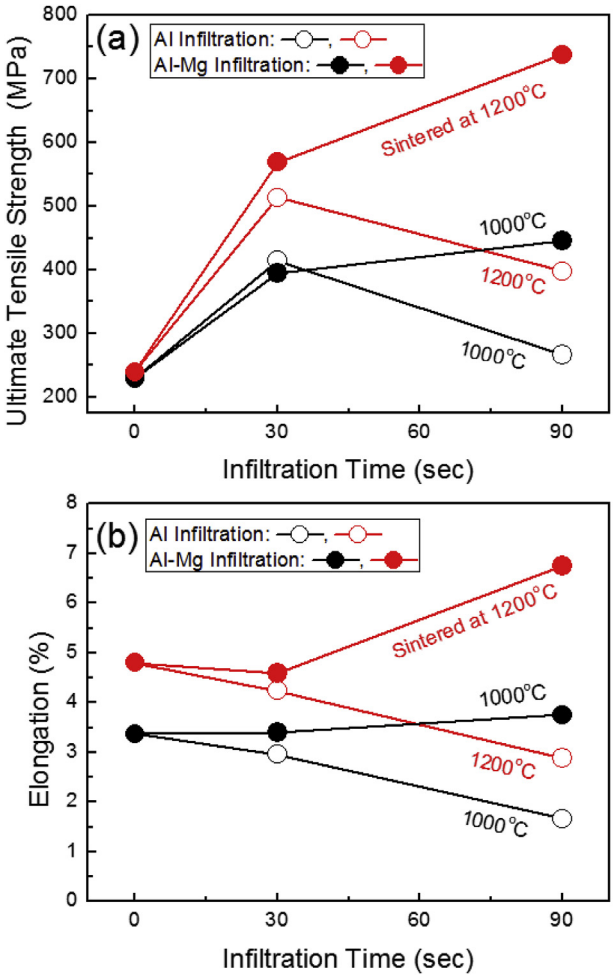

Fig. 14. Mechanical properties, including (a) ultimate tensile strength and (b) elongation of the as-infiltrated samples infiltrated with Al [from Fig. 6(b)] and with Al-Mg (from Fig. 11).

4. Conclusions

We present an efficient process combining powder injection molding (MIM) and infiltration of second and/or third elements to fabricate in-situ strengthened Ti composites. The porous Ti compacts were prepared by MIM with various sintering temperatures. Molten Al or Al-Mg was infiltrated into the pores of the Ti compacts for 30–90 s. In the case of Al infiltration, $TiAl_3$ was produced as the reaction product between solid Ti and molten Al. Post-heat treatment processing was applied after infiltration to ensure homogeneity and to promote the growth of desirable phases. However, the high-temperature heat treatment resulted in voids that severely degraded the mechanical properties of the composite. The generation of voids was explained by the melting/evaporation of Al, the Kirkendall effect, and the difference in molar volumes among the different phases formed. The main cause of strength deterioration was the extensive formation of brittle $TiAl_3$ even in the early stages of infiltration. To circumvent this problem, an approach was employed in this study to use Al(Mg) alloy for the infiltration of the porous Ti compacts. The Mg added to the Al readily forms an Al(Mg) solid solution inside the pores and this effectively prevents the formation and growth of $TiAl_3$. As a result, by a simple process of infiltrating second and/or third elements into the pores of pure Ti for short times (30–90 s), we can obtain in-situ reinforced Ti

composites having near-net shape with higher strength and elongation. This may provide a simple and effective route to fabricate complex shaped Ti-based parts having good mechanical properties.

Acknowledgements

This work was supported by the Korea government (MSIP) (NRF-2013R1A1A2004989, 2014R1A2A1A10053869), and the Priority Research Centers Program (2009-0093823) through the National Research Foundation of Korea (NRF).

References

[1] C. Leyens, M. Peters, Titanium and Titanium Alloys, Wiley-VCH, 2001.
[2] K. Faller, F.H. Froes, The use of titanium in family automobiles: current trends, JOM 53 (2001) 27.
[3] Ma Qian, Francis H. Froes, Titanium Powder Metallurgy, Butterworth-Heinemann, 2015.
[4] G. Shibo, D. Bohua, H. Xinbo, Q. Xuanhui, Powder injection molding of pure titanium, Rare Met. 28 (2009) 261.
[5] E. Nyberg, M. Miller, K. Simmons, K.S. Weil, Microstructure and mechanical properties of titanium components fabricated by a new powder injection molding technique, Mater. Sci. Eng. C 25 (2005) 336–342.
[6] O. Ivasishin, V. Moxson, Titanium Powder Metallurgy: Science, Technology and Applications, Elsevier, 2015.
[7] E. Carreño-Morelli, W. Krstev, B. Romeira, M. Rodriguez-Arbaizar, J.-E. Bidaux, S. Zachmann, Powder Injection Moulding of Titanium from TiH_2 Powders, Euro PM2009, 2, p 9–14.
[8] W.S. Chang, B.C. Muddle, Trialuminide intermetallic alloys for elevated temperature applications – overview, Met. Mater. Int. (1997) 1–15.
[9] D.M. Dimiduk, D.B. Mirade, High-temperature Ordered Intermetallic Alloys III, MRS, 1989, p. p 349.
[10] T. Ebel, C. Blawert, R. Willumeit, B.J.C. Luthringer, O.M. Ferri, F. Feyerabend, Ti–6Al–4V–0.5B–A modified alloy for implants produced by metal injection molding, Adv. Eng. Mater. (2011) 13.
[11] W.Y. Jeung, Powder injection molding and magnetic material, Bul. Kor. Inst. Met. Mater. (1999) 12.
[12] K. Honda, M. Sugiyama, Y. Ikematsu, K. Ushioda, Role of $TiAl_3$ fine precipetate in nucleation of the primary Al dendrite phase during solidification in hot-dip Zn-11% Al-3% Mg-0.2% Si coated steel sheet, Mater. Trans. 52 (2011) 90–95.
[13] Y. Wei, W. Aiping, Z. Guisheng, R. Jialie, Formation process of the bonding joint in Ti/Al diffusion bonding, Mater. Sci. Eng. A 480 (2008) 456–463.
[14] U.R. Kattner, J.C. Lin, Y.A. Chang, Thermodynamic assessment and calculation of the Ti-Al system, Metall. Mater. Trans. A 23 (1992) 2081.
[15] R. Orru, G. Cao, Z.A. Munir, Mechanistic investigation of the field-activated combustion synthesis (FACS) of titanium aluminides, Chem. Eng. Sci. 54 (1999) 3349–3355.
[16] L. Xu, Y.Y. Cui, Y.L. Hao, R. Yang, Growth of intermetallic layer in multi-laminated Ti/Al diffusion couples, Mater. Sci. Eng. A 435–436 (2006) 638–647.
[17] H. Fukutomi, M. Nakamura, T. Suzuki, S. Takagi, S. Kikuchi, Void formation by the reactive diffusion of titanium and aluminum foils, Mater. Trans. 41 (2000) 1244–1246.
[18] Y. Jiang, C. Deng, Y. He, Y. Zhao, N. Xu, J. Zou, B. Huang, C.T. Liu, Reactive synthesis of microporous titanium-aluminide membranes, Mater. Lett. 63 (2009) 22–24.
[19] Y. Sun, Y. Zhao, D. Zhang, C. Liu, H. Diao, C. Ma, Multilayered Ti-Al intermetallic sheets fabricated by cold rolling and annealing of titanium and aluminum foils, Trans. Nonferrous Met. Soc. China 21 (2011) 1722–1727.
[20] H.C. Yi, A. Petric, J.J. Moore, Effect of heating rate on the combustion synthesis of Ti-AI intermetallic compounds, J. Mater. Sci. 27 (1992) 6797–6806.
[21] K. Kondoh, M. Kawakami, H. Imai, H. Umeda, H. Fujii, Wettability of pure Ti by molten pure Mg droplets, Acta Mater. 5 (2010) 606–614.
[22] I.N. Frantsevich, D.M. Karpinos, L.I. Tuchinskii, A.B. Sapozhnikova, L.N. Klimenko, Kinetics of infiltration of porous titanium magnesium, Powder Metall. Met. Ceram. 16 (1977) 534–537.